Biosensors and Bioelectronics 68 (2015) 429–436

Contents lists available at ScienceDirect

Biosensors and Bioelectronics

journal homepage: www.elsevier.com/locate/bios

Cyclodextrin functionalized graphene–gold nanoparticle hybrids with strong supramolecular capability for electrochemical thrombin aptasensor

Qiong Xue [a], Zhiguang Liu [a], Yujing Guo [a,*], Shaojun Guo [b]

[a] Institute of Environmental Science, College of Chemistry and Chemical Engineering, Shanxi University, Taiyuan 030006, China
[b] Physical Chemistry and Applied Spectroscopy, Los Alamos National Laboratory, Los Alamos, NM 87545, USA

ARTICLE INFO

Article history:
Received 20 September 2014
Received in revised form
9 January 2015
Accepted 10 January 2015
Available online 12 January 2015

Keywords:
Graphene
Thio-β-cyclodextrin
Gold nanoparticle
Aptasensor
Supramolecular recognition

ABSTRACT

We demonstrate a facile one-pot synthetic strategy for controlled synthesis of thio-β-cyclodextrin functionalized graphene/gold nanoparticles (SH-β-CD-Gr/AuNPs) composites using SH-β-CD as both the dispersant and linker. The obtained SH-β-CD-Gr/AuNPs integrate the excellent electrical properties and large surface area of graphene and AuNPs with supramolecular recognition ability of CD, which show more effective electron transfer and higher enriched ability for the ferrocene probe via the host–guest interaction between CD and ferrocene than SH-β-CD-Gr. In the presence of target, the stronger interaction between aptamer and target makes the ferrocene move closer to the electrode surface, thus facilitating the electron transfer. Based on this sensing mechanism, a new and highly sensitive biosensing concept by the use of SH-β-CD-Gr/AuNPs as enhancing materials is demonstrated for "signal-on" detection of targets (thrombin as a model target). This biosensor exhibits a wide linear range for thrombin from 1.6×10^{-17} M to 8.0×10^{-15} M and a very low limit of detection 5.2×10^{-18} M, which is two-order magnitude better than those of SH-β-CD-Gr (the detection linear range from 1.6×10^{-15} M to 8.0×10^{-13} M and detection limit of 1.0×10^{-15} M). Our proposed electrochemical aptasensor based on SH-β-CD-Gr/AuNPs shows good selectivity against other proteins such as human serum albumin, lysozyme and insulin. To the best of our knowledge, the present SH-β-CD-Gr/AuNPs hybrids are the most efficient graphene-based electrochemical active probes ever reported for biosensors.

1. Introduction

The development of simple, ultrasensitive, highly selective and cost-effective biosensing platforms is essential for biological assays and clinical diagnostics. Due to their unique physicochemical properties, nanomaterials possess the good ability to facilitate the signal transduction and amplify the molecular recognition events (Rosi and Mirkin, 2005; Saha et al., 2012; Wang et al., 2009), which makes them ideal candidates in the design of biosensing systems with advanced functions. Among different existed nanomaterials, graphene can functionalize as an excellent transducing element due to their fascinating physical and chemical characteristics (Chen et al., 2012; Feng et al., 2013; Loh et al., 2010). It has been largely exploited to develop the improved chemical and biological electrochemical sensors to detect some important biomolecules (Zhou et al., 2009; Shang et al., 2008; Choi et al., 2010) and small molecules (Wu et al., 2010; Fang et al., 2010), and also high performance field-effect transistor biosensors in detecting different gas molecules (Schedin et al., 2007; Robinson et al., 2008; Joshi et al., 2010) and biomolecules (Kim et al., 2013; Ohno et al., 2009; Chen et al., 2013). It can also work as a super quencher to strongly quench the fluorescence of dyes and quantum dots when they are close to each other, and based on this principle, graphene-based fluorescent sensors for the detection of different targets (Guo and Dong, 2011) are becoming popular. Graphene also shows the strong peroxidase-like catalytic ability, which has been utilized to develop colorimetric sensors by catalyzing the oxidation of the substrate 3,3,5,5 -tetramethylbenzidine (TMB) or 2,2-azino-bis(3-ethylbenzothiazoline-6-sulfonic acid) ($ABTS^{2-}$) in the presence of H_2O_2 to colored product (Song et al., 2010; Y. Guo et al., 2011; Y.J. Guo et al., 2011; Tao et al., 2013).

Among the various sensing platforms, graphene based electrochemical sensors are of more particular interest due to the advantages of high sensitivity, intrinsic simplicity, low cost and the potential for miniaturization. And a number of reports have been dedicated to the development of graphene and graphene-related materials for the electrochemical analysis of important molecules. Despite the attractive features in enhancing the detection ability

* Corresponding author. Fax: +86 351 7011011.
E-mail address: guoyj@sxu.edu.cn (Y. Guo).

http://dx.doi.org/10.1016/j.bios.2015.01.025
0956-5663/

for the target of interest, graphene itself still shows the limited detection sensitivity. In this regard, the development of graphene-based composite for high-sensitivity sensors has been in flourish in the last two years. Particularly, recent significant advances reveal that the clever combination of graphene with metal nanoparticles (NPs), leading to the development of a multicomponent nanoassembly system, opens a new avenue for utilizing graphene-based hybrid nanomaterials as enhanced elements for constructing new electrochemical sensing platform with high performance (S. Guo et al., 2011).

Cyclodextrins (CDs) are well-known materials for forming the inclusion complexes with various guest molecules because of their molecular structure containing a hydrophobic internal cavity and hydrophilic external surface (Rekharsky and Inoue, 1998; Wang and Khaledi, 1996). By composing graphene with CDs, we demonstrated a wet-chemical process for the synthesis of CD-functionalized graphene nanosheets with high supramolecular recognition and enrichment capability, which show much higher electrochemical performance towards eight probe molecules (biomolecules and drugs) than unmodified graphene and carbon nanotubes (Guo et al., 2010). Tian et al. (2012) use AuNPs–β-CD-graphene modified glassy carbon electrode (GCE) for the simultaneous determination of AA, DA and UA with satisfactory results. By extending our system to graphene–metal NPs hybrids, herein, we developed a facile yet simple one-pot synthesis of thio-β-cyclodextrin functionalized graphene–gold NPs composites (SH-β-CD-Gr/AuNPs) using SH-β-CD as both the dispersant and linker. We found that SH-β-CD had better advantage than individual β-CD in obtaining good-quality SH-β-CD-Gr/AuNPs. Totally different from our previous CD-Gr system, by integrating the better electrical properties and larger specific surface area of graphene and AuNPs, the SH-β-CD-Gr/AuNPs hybrids can more effectively accelerate the electron transfer and enrich more CDs than graphene, which is very necessary for binding more ferrocene by the host and guest interactions. Specially, the results from electrochemistry obviously reveal that SH-β-CD-Gr/AuNPs exhibit much stronger enriched capability than SH-β-CD-Gr and show higher electrochemical performance towards ferrocene. This is very important for further enhancing the electrochemical signal probe for high sensitivity aptasensors.

As is known, thrombin is a proteolytic enzyme for facilitating the blood clotting by converting fibrinogen into fibrin and regarded as a tumor marker in the diagnosis of pulmonary metastasis (Nierodzik and Karpatkin, 2006). And aptamer–thrombin is a well-known system for constructing biosensors for thrombin detection by the use of electrochemical, colorimetric and optical signals, etc. (Tombelli et al., 2005; Song et al., 2008; Liu et al., 2009; Zhao et al., 2011). Recently, some elegant electrochemical aptasensor strategies have been designed for the sensitive detection of thrombin using graphene related material. For example, Our group proposed a label-free electrochemical protocol for "signal-on" detection of thrombin with the low detection limit of 3.5×10^{-13} M based on electroactive dye-Orange II functionalized graphene nanosheets (Guo et al., 2013). Zhang et al. (2013) reported an electrochemical thrombin aptasensor with a low detection limit of 9.3×10^{-11} M based on gold nanoparticles/thionine–graphene nanocomposite modified glassy carbon electrode. Based on the strong specific interaction between aptamer and the target molecule, herein we select the aptamer–thrombin system as a model biosensing platform to demonstrate the advantage of SH-β-CD-Gr/AuNPs. As a result, our newly designed SH-β-CD-Gr/AuNPs hybrids can be used as very high-sensitivity probe for the detection of thrombin with a wide linear range of 1.6×10^{-17} M to 8.0×10^{-15} M and a very low detection limit of 5.2×10^{-18} M, which is much better than that of SH-β-CD-Gr (the detection linear range from 1.6×10^{-15} M to 8.0×10^{-13} M and detection limit of 1.0×10^{-15} M). To the best of our knowledge, the present SH-β-CD-Gr/AuNPs hybrids are the most efficient graphene-based electrochemical active probes ever reported for biosensors.

2. Experimental section

2.1. Reagents and Instruments

Graphite was purchased from Alfa Aesar. SH-β-CD was purchased from Shangdong Binzhou Zhiyuan Biotechnology Company. Hydrazine solution (50 wt%) and ammonia solution (25–28 wt%) were obtained from Beijing Chemical Reagent Company (Beijing, China). $HAuCl_4 \cdot 4H_2O$ was obtained from Shanghai Chemical Factory. Ferrocene modified thrombin binding aptamer (Fc-TBA): 5′-GGT TGG TGT GGT TGG-Fc-3′, was purchased from Sangon Inc. (Shanghai, China). Human serum albumin (HAS), bovine serum albumin (BSA), lysozyme, and insulin were obtained from Sigma Co. TE buffer (10 mM Tris–HCl, 0.1 M NaCl and 1 mM EDTA, pH 6.0) was used as a binding buffer. Tris–HCl buffer (20 mM Tris–HCl, 0.1 M NaCl and 5.0 mM $MgCl_2 \cdot 6H_2O$, pH 7.0) was used as a working buffer. Water used throughout all experiments was purified with the Millipore system.

UV–vis absorption spectra were recorded on a U-3010 spectrometer (Hitachi, Ltd., Tokyo, Japan). Fourier transform infrared (FTIR) spectra were recorded on a Shuimadzu 8400S spectrometer (Shimadzu, Japan). Transmission electron microscopy (TEM) images were obtained with a JEM-1011 transmission electron microscope operating at 100 kV. X-ray photoelectron spectroscopy (XPS) measurement was performed on an ESCALAB-MKII 250 photoelectron spectrometer (VG Co.) with Al Kα X-ray radiation as the X-ray source for excitation. Electrochemical measurements were carried out on a CHI660C electrochemical workstation (Chenhua Instruments Co., Shanghai, China). A three-electrode system was used in the experiment with the glassy carbon electrode (GCE, 3 mm diameter) as working electrode, a saturated calomel electrode (SCE) and a Pt wire electrode were used as reference and counter electrodes, respectively.

2.2. Preparation of SH-β-CD-GR/AuNPs and SH-β-CD-Gr

Graphene oxide (GO) was synthesized from natural graphite by the previous protocol with a modification on Hummers' method (Hummers and Offeman, 1958). SH-β-CD-Gr/AuNPs was prepared as follows: 2.5 mL of 4 mg/mL SH-β-CD aqueous solution was first mixed with 1.25 mL of 1.0 mg/mL GO and 300 μL of ammonia solution. Then, 250 μL of 24.3 mM $HAuCl_4$ and 20 μL of hydrazine solution were added into the flask. After being vigorously stirred for a few minutes, the flask was put in a water bath (60 °C) for 3.5 h, a stable black dispersion was obtained. After that, the mixture was filtered with a Nylon membrane (0.22 μm) to obtain SH-β-CD-Gr/AuNPs that can be redispersed readily in water by ultrasonication. Additionally, the preparation of SH-β-CD-Gr was similar with SH-β-CD-Gr/AuNPs hybrids except no addition of $HAuCl_4$.

2.3. Fabrication of the sensing interface

GCE was polished to a mirror-like surface and rinsed thoroughly with doubly distilled water and dried in air. Then, 7.0 μL of 0.31 mg/mL SH-β-CD-Gr/AuNPs was dropped on the surface of GCE and dried at room temperature to obtain SH-β-CD-Gr/AuNPs modified GCE (SH-β-CD-Gr/AuNPs/GCE). After that, 5.0 μL of 5.0 mM Fc-TBA (dispersed in TE buffer) was dropped on the surface of the SH-β-CD-Gr/AuNPs/GCE and stored at 4 °C overnight to obtain the sensing interface of Fc-TBA/SH-β-CD-Gr/AuNPs/GCE

2.4. Electrochemical detection of thrombin

The as-prepared sensing interface was immersed into 20 mM Tris–HCl (pH, 6.0) buffer solution containing thrombin with different concentrations and incubated for 60 min. Then, the differential pulse voltammetry (DPV, a very sensitive electrochemical detection technique) signals of ferrocene under different concentrations of thrombin were collected with the instrumental parameters: pulse width 0.05 s, pulse period 0.2 s and pulse amplitude of 5 mV.

3. Results and discussion

3.1. The protocol of the biosensor

The schematic procedure for the synthesis of SH-β-CD-Gr/AuNPs and our sensing concept for enhancing the electrochemical thrombin detection by the use of SH-β-CD-Gr/AuNPs with higher supramolecular recognition ability (A) than SH-β-CD-Gr (B) are shown in Scheme 1. Firstly, a simple wet-chemical route is employed for synthesizing SH-β-CD-Gr/AuNPs through the heating reduction of graphene oxide in the presence of hydrazine. During the reaction period, SH-β-CD not only serves as a stabilizer for the formation of AuNPs due to the strong Au–S bonds (Filippini et al., 2014) but also as a bifunctional linker to connect AuNPs onto graphene by forming hydrogen bonds between graphene and hydroxyl groups of SH-β-CD (Guo et al., 2010). Then, Fc-TBA is attached onto the SH-β-CD-Gr/AuNPs/GCE through host–guest recognition between ferrocene labeled TBA and CDs in order to obtain the sensing interface of Fc-TBA/SH-β-CD-Gr/AuNPs/GCE. After immersing the sensing interface into the target solution, the aptamer can recognize the target, making the ferrocene move closer to the electrode surface, thus making the electron transfer faster. This strategy combine the unique properties of the Gr–AuNPs, cyclodextrin and aptamer, making our SH-β-CD-Gr/AuNPs based sensing platform among the best electrochemical sensing ones.

3.2. Characterization of SH-β-CD-GR/AuNPs

Fig. 1A displays the UV–vis absorption spectra of GO (a) and SH-β-CD-Gr/AuNPs (b). The absorption spectrum of GO shows a characteristic peak at 229 nm owing to the π–π* transition of aromatic C=C bonds and a shoulder at 290–300 nm corresponding to the n–π* transition of the C=O bond (Ang et al., 2009) (curve a). After introducing SH-β-CD and $HAuCl_4$ into the GO solution and further reduced by hydrazine, the absorption peak of 229 nm significantly red shifts to 269 nm and their absorbance in the whole spectral region also increases, suggesting that the electronic conjugation within the graphene is restored by hydrazine (Li et al., 2008). Meanwhile, a new obvious absorption peak at 569 nm appears, confirming that $HAuCl_4$ is reduced to AuNPs (Orendorff et al., 2006). The FT-IR spectra (Fig. 1B) of graphene (a), SH-β-CD (b) and SH-β-CD-Gr/AuNPs (c) also provide a clear evidence for the successful functionalization of SH-β-CD onto Gr–AuNPs hybrids. The FT-IR spectrum of graphene is essentially featureless except the C=C conjugation (1550 cm^{-1}) and C–C band (1190 cm^{-1}), etc. Whereas the FT-IR spectrum of SH-β-CD-Gr/AuNPs (curve c) exhibits typical SH-β-CD absorption features (curve b) of the ring vibrations at 578, 703, 756 and 937 cm^{-1}, the coupled C–O/C–C stretching bending vibrations at 1027 cm^{-1}, CH_2 stretching vibrations at 2925 cm^{-1}, and O–H stretching vibrations at ~3390 cm^{-1}. The disappearance of the absorption features of –SH stretching vibrations at ~2575 cm^{-1} verifies the formation of Au–S bond.

The formation of SH-β-CD-Gr/AuNPs is further characterized by energy-dispersive X-ray photoelectron spectroscopy (XPS). As shown in Fig. 1C–F, the XPS result of SH-β-CD-Gr/AuNPs shows the obvious Au4f and S2p peaks originating from AuNPs and SH-β-CD, respectively. The magnified images further show that the significant Au4f signals correspond to the binding energy of Au and S signal coming from the binding energy of S (originate from SH-β-CD). All the above data prove that SH-β-CD molecules are effectively attached onto the surface of SH-β-CD-Gr/AuNPs.

The as-prepared SH-β-CD-Gr–AuNPs can be easily dispersed in water. Fig. 2 shows the typical TEM images of SH-β-CD-Gr (Fig. 2A) and SH-β-CD-Gr/AuNPs hybrids (Fig. 2B, C). Two-dimensional flake-like morphology with wrinkled topology is observed in SH-

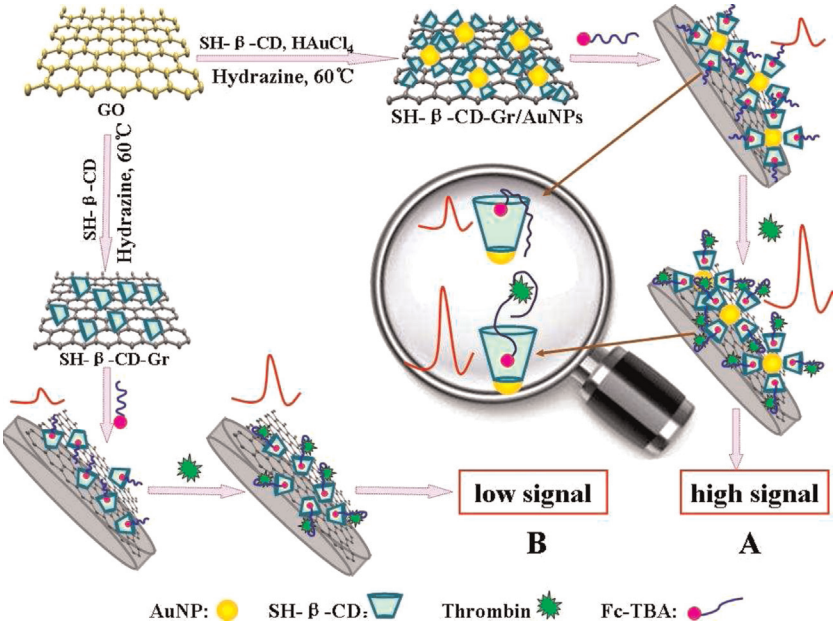

Scheme 1. Schematic procedure for the synthesis of SH-β-CD-Gr/AuNPs and our sensing concept for enhancing the electrochemical thrombin detection by the use of SH-β-CD-Gr/AuNPs with higher supramolecular recognition ability (A) than SH-β-CD-Gr (B).

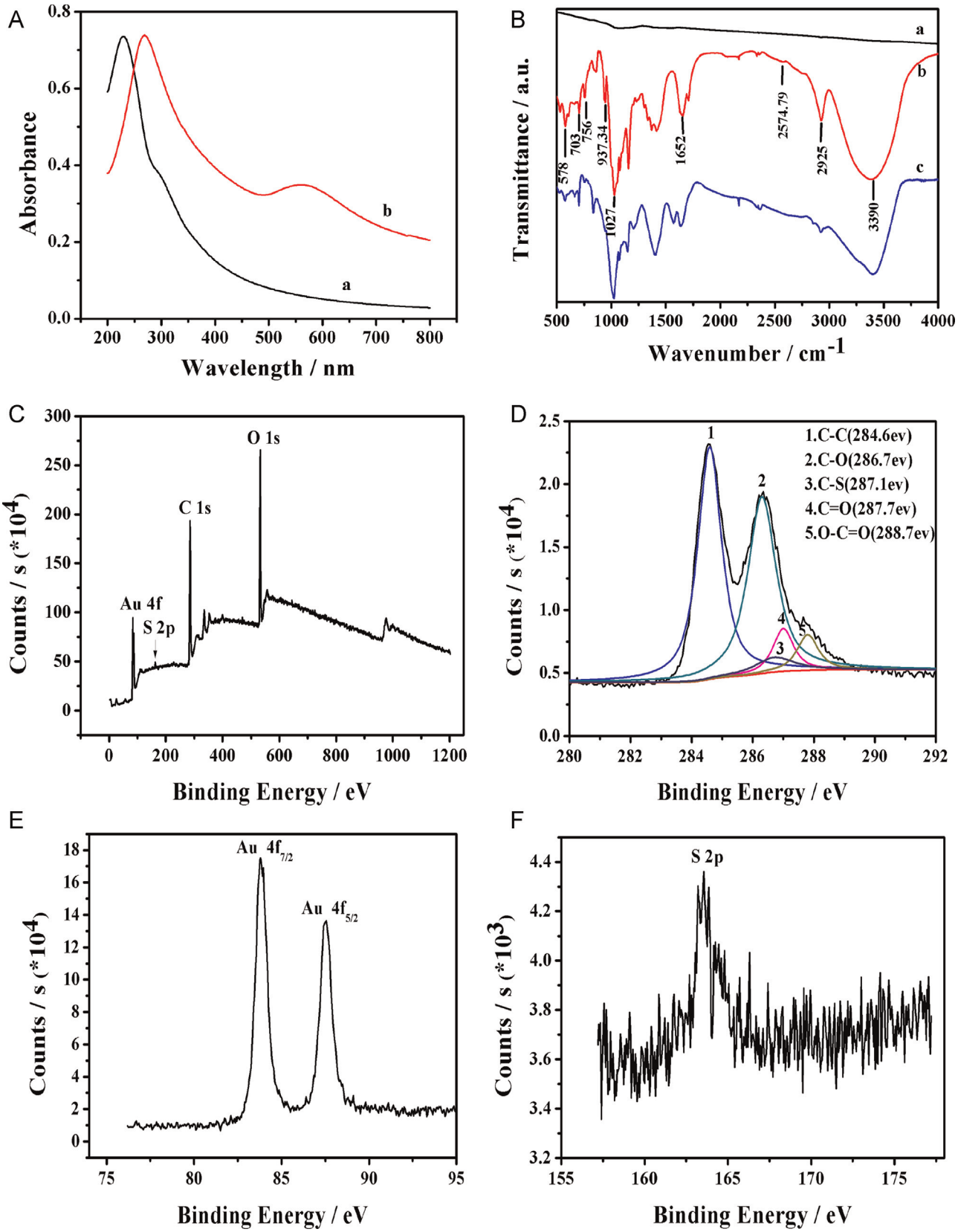

Fig. 1. (A) UV–vis spectra of GO (a) and SH-β-CD-Gr/AuNPs (b); (B) FT-IR spectra of graphene (a), SH-β-CD (b) and SH-β-CD-Gr/AuNPs (c). (C) Survey XPS spectra of SH-β-CD-Gr/AuNPs; (D–F): XPS of SH-β-CD-Gr/AuNPs: (D) C1s (E) Au4f; (F) S2p.

β-CD-Gr, being in accordance with the structure of single-layer graphene (Guo et al., 2009). As for the SH-β-CD-Gr/AuNPs hybrids, a totally different morphology is observed, in which a lot of small AuNPs are uniformly distributed on the surface of the graphene. The size of AuNPs is determined to be from 10 to 18 nm (Fig. 2D). Here, both graphene and AuNPs can be modified with

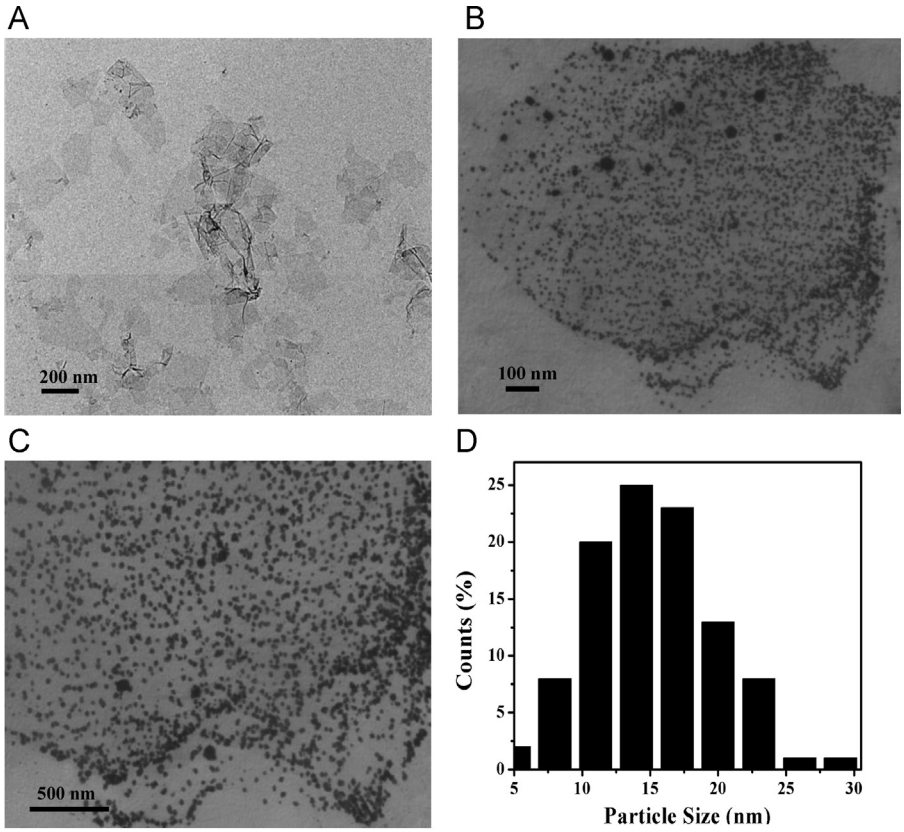

Fig. 2. TEM images of SH-β-CD-Gr (A) and SH-β-CD-Gr/AuNPs at different magnifications (B, C). (D) The size distribution of AuNPs on SH-β-CD-Gr.

cyclodextrins, which can provide more sites for ferrocene attachment through forming stable host–guest complex between CD and ferrocene. This is very important for amplifying the electrochemical signal and improving the sensitivity of the present sensing system.

3.3. *Electrochemical detection of thrombin by differential pulse voltammetry (DPV)*

DPV was used to monitor the signal change of ferrocene on the Fc-TBA/SH-β-CD-Gr/AuNPs/GCE in the presence and absence of thrombin. As shown in Fig. 3, there is no peak on the DPV curve of SH-β-CD-Gr/AuNPs/GCE in the potential range (curve a). But after Fc-TBA is covered on the SH-β-CD-Gr/AuNPs/GCE surface, an obvious peak located at 0.49 V vs. SCE appear, which can be attributed to the oxidation of ferrocene enriched on the surface of the electrode according to the host–guest interaction between CD and ferrocene (curve c). The peak current of ferrocene on SH-β-CD-Gr/AuNPs/GCE is bigger than that on the SH-β-CD-Gr/GCE (curve b), because there are more CDs covered on the surface of SH-β-CD-Gr/AuNPs. Therefore, more ferrocene can be enriched on the surface of SH-β-CD-Gr/AuNPs, resulting in a larger response signal. When the as-prepared sensing interfaces are immersed into thrombin solution and incubated for 60 min, the peak current increases. This is because in the presence of thrombin, the formed TBA–thrombin complex make the label part of TBA (ferrocene) move more closer to the electrode surface, thus facilitating the electron transfer and resulting in signal increase (Fig. 3 curve d).

To achieve the better sensing performance, some important parameters have been optimized. Firstly, the influence of pH values on the electrochemical behavior was first investigated. The Fc-TBA/SH-β-CD-Gr/AuNPs/GCE sensing interface was immersed in

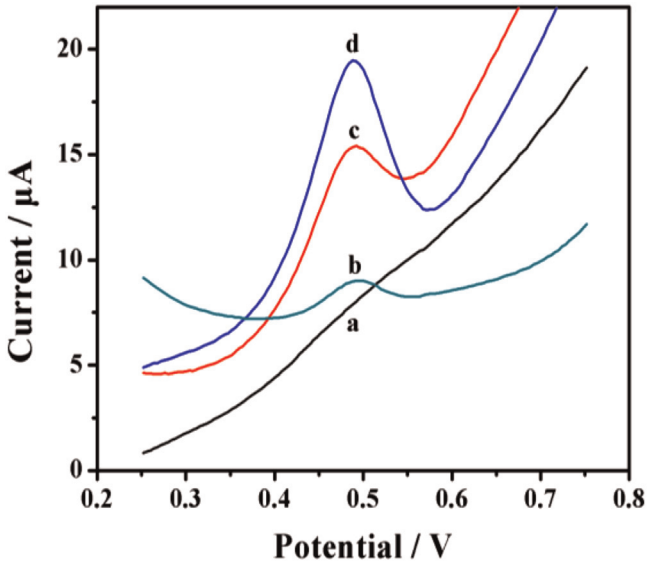

Fig. 3. DPV of different modified electrodes: SH-β-CD-Gr/AuNPs/GCE (a); Fc-TBA–SH-β-CD-Gr/GCE (b); Fc-TBA–SH-β-CD-Gr/AuNPs/GCE (c) and Fc-TBA–SH-β-CD-Gr/AuNPs/GCE incubated in 1.6×10^{-16} M thrombin solution (d).

Tris–HCl buffer solution with different pH values containing 1.6×10^{-16} M thrombin and DPV signals were recorded, respectively. As shown in Fig. 4A, the peak current reaches to the maximum at pH 6.0. Therefore, pH 6.0 Tris–HCl is used as the supporting electrolyte in all voltammetric determinations. Then, the effect of the amount of SH-β-CD-Gr/AuNPs on the electrochemical performance was investigated. As shown in Fig. 4B, the peak currents increase remarkably when the amount of SH-β-CD-Gr/AuNPs

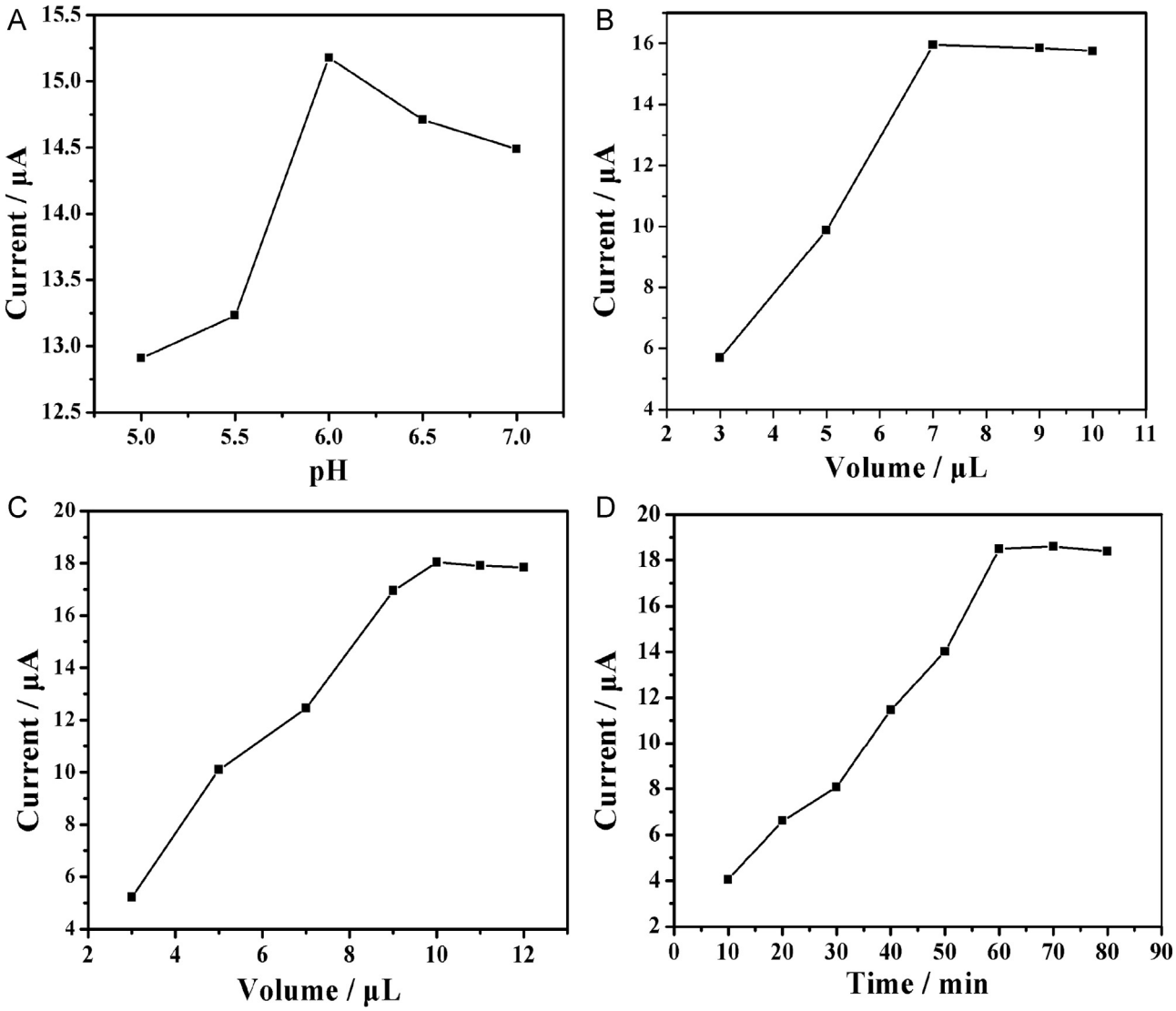

Fig. 4. (A) The effect of the pH values on the peak current; (B) the effect of the amounts of SH-β-CD-Gr/AuNPs on the peak current; (C) the effect of the modified volume of Fc-TBA on the peak current; (D) the relationship between the peak current and the incubate time. All the experiments have been done in Tris–HCl buffer solution containing 1.6×10^{-16} M thrombin.

suspension (0.31 mg/mL) increases from 3.0 to 7.0 μL. However, when the amount of SH-β-CD-Gr/AuNPs exceeds 7.0 μL, the peak current has a slight decrease. Consequently, a 7.0 μL of 0.31 mg/mL SH-β-CD-Gr/AuNPs suspension was selected as the optimum volume for modification of the GCE. We also studied the effect of the amount of Fc-TBA modified on the SH-β-CD-Gr/AuNPs/GCE on the electrochemical performance, as shown in Fig. 4C. It is observed that the peak current increases with the amount of Fc-TBA from 3.0 to 10 μL, and keeps nearly constant after 10 μL more. Herein, 10 μL of 5.0 mM Fc-TBA was used to modify the SH-β-CD-Gr/AuNPs/GCE. Lastly, the relationship between the peak current and the incubate time was investigated (Fig. 4D). The DPV signal increases significantly with the increase of thrombin binding time, and a plateau is achieved after the incubation time for over 60 min. Therefore, a hybridization time of 60 min was adopted in the following experiments.

Because the DPV signal of ferrocene was dependent on the existence of the thrombin, it was used to indicate and quantify the target. As shown in Fig. 5A, the increased DPV signals are directly related to the concentration of thrombin. There is a linear relationship between the current and logarithmic thrombin concentration from 1.6×10^{-17} M to 8.0×10^{-15} M with a correlation coefficient of 0.9762 (Fig. 5B), and the detection limit of thrombin is 5.2×10^{-18} M using the signal (S) to noise ratio (N) $S/N=3$. In contrast, the linear range for the detection of thrombin on the SH-β-CD-Gr/GCE is from 1.6×10^{-15} M to 8.0×10^{-13} M and the detection limit is 1.0×10^{-15} (Fig. 5C, D). The analytical performance of the SH-β-CD-Gr/AuNPs based aptasensor for thrombin detection is also compared with the reported results based on electrochemical nanoprobes in the literature (Table S1) (H.Y. Bai et al., 2013; Xu et al., 2013; L. Bai et al., 2013; Wu et al., 2013). It is obvious that our proposed aptasensor based on SH-β-CD-Gr/AuNPs exhibits a much higher sensitivity for highly sensitive detection of thrombin. These results reveal that the SH-β-CD-Gr/AuNPs hybrids as matrices not only increase the immobilization of ferrocene, but also facilitate the electron transfer between ferrocene and the electrode surface.

3.4. The selectivity, stability and reproducibility of the present sensing interface

To assess the selectivity of the immobilized aptamer for thrombin over other proteins, the sensing interfaces were immersed into

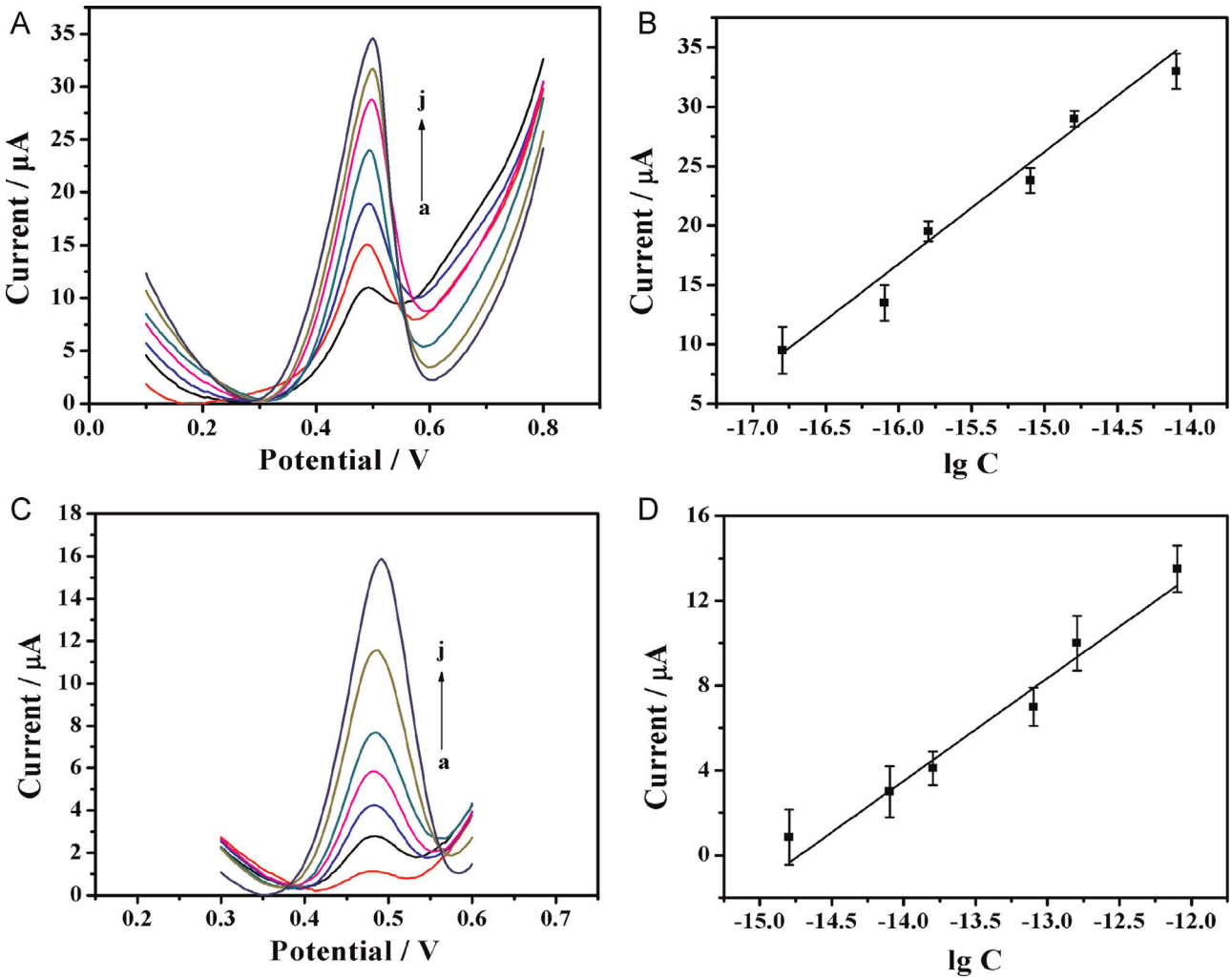

Fig. 5. (A) The DPV of the sensing interface at different concentrations of thrombin using the Fc-TBA–SH-β-CD-Gr/AuNPs/GCE. From a to j: 0, 1.6×10^{-17}, 8.0×10^{-17}, 1.6×10^{-16}, 8.0×10^{-16}, 1.6×10^{-15}, 8.0×10^{-15} M. (B) The calibration curve between the current response and the thrombin concentration (logarithm). The measurements were repeated 3 times to obtain the standard deviation. (C) The DPV of the sensing interface at different concentrations of thrombin using the Fc-TBA–SH-β-CD-Gr/GCE. From a to j: 0, 1.6×10^{-15}, 8.0×10^{-15}, 1.6×10^{-14}, 8.0×10^{-14}, 1.6×10^{-13}, 8.0×10^{-13} M. (D) The calibration curve between the current response and the thrombin concentration (logarithm). The measurements were repeated 3 times to obtain the standard deviation.

1.6×10^{-16} M thrombin, BSA, HSA, lysozyme, and insulin, and further incubated for 60 min, respectively. As expected, there is a nearly negligible signal change toward HSA, lysozyme and insulin. However, it is clearly observed that the peak current of ferrocene increases significantly with thrombin (Fig. S1). The experimental results demonstrate that the proposed strategy has a satisfactory selectivity for thrombin detection. This excellent specificity arises from the highly specific binding affinity of the anti-thrombin aptamers.

To investigate the stability of the aptasensor, the as-prepared sensing interface was stored in ultrapure fresh water at 4 °C over 2 weeks and then recovered to room temperature slowly. The response current of the biosensor decreases only about 4.3% of the initial values, illustrating the present SH-β-CD-Gr/AuNPs-based biosensor has a good stability. The reproducibility of this aptasensor was also investigated. The seven sensing interfaces based on SH-β-CD-Gr/AuNPs were used to detect thrombin with the same concentration (1.6×10^{-16} M) under the same condition. The relative standard deviation (RSD) is 5.7%, suggesting the proposed aptasensor has an acceptable reproducibility for the detection of thrombin.

4. Conclusions

To summarize, we report one-pot synthesis of SH-β-CD-Gr/AuNPs using simple wet chemical strategies and also demonstrate their good ability as a highly sensitive sensing platform for ultrasensitive electrochemical detection of thrombin based on the host–guest interaction between CD and ferrocene modified aptamer. SH-β-CD-Gr/AuNPs can not only facilitate the electrons transfer but also provide a large accessible surface area for loading large amount of CDs and immobilizing abundant of Fc-TBA, thus amplifying the response signals and improving the sensitivity. The detection limit is two-order magnitude lower than those of SH-β-CD-Gr for thrombin determination. The resulting aptasensor exhibits superior performance such as low detection limit, acceptable stability and reproducibility. Considering the high detection sensitivity, broad target applicability and easy to fabricate, we expect that the described biosensing platform will find wide applications in biological, medical, and environmental fields.

Acknowledgements

This research work was supported by the National Natural Science Foundation of China (No. 21275093), the Natural Science Foundation of Shanxi Province (No. 2012011007-3) and the Program for the Outstanding Innovative Teams of Higher Learning Institutions of Shanxi, 2013 (No. 2013803).

Appendix A. Supplementary material

Supplementary data associated with this article can be found in the online version at http://dx.doi.org/10.1016/j.bios.2015.01.025.

References

Ang, P.K., Wang, S., Bao, Q., Thong, J.T.L., Loh, K.P., 2009. ACS Nano 3, 3587–3594.
Bai, H.Y., Campo, F., Tsai, Y.C., 2013. Biosen. Bioelectron. 42, 17–22.
Bai, L., Chai, Y., Yuan, R., Yuan, Y., Xie, S., Jiang, L., 2013. Biosen. Bioelectron. 50, 325–330.
Choi, B.G., Park, H., Park, T.J., Yang, M.H., Kim, J.S., Jang, S.-Y., Heo, N.S., Lee, S.Y., Kong, J., Hong, W.H., 2010. ACS Nano 4, 2910–2918.
Chen, D., Feng, H., Li, J.H., 2012. Chem. Rev. 112, 6027–6053.
Chen, T.Y., Loan, P.T., Hsu, C.L., Lee, Y.H., Tse-Wei Wang, J., Wei, K.H., Lin, C.T., Li, L.J., 2013. Biosens. Bioelectron. 41, 103–109.
Fang, Y., Guo, S., Zhu, C., Zhai, Y., Wang, E., 2010. Langmuir 26, 11277–11282.
Feng, L.Y., Wu, L., Qu, X.G., 2013. Adv. Mater. 25, 168–186.
Filippini, G., Goujon, F., Bonal, C., Malfreyt, P., 2014. J. Phys. Chem. C 118, 3102–3109.
Guo, H.L., Wang, X.F., Qian, Q.Y., Wang, F.B., Xia, X.H., 2009. ACS Nano 3, 2653–2659.
Guo, S., Dong, S., 2011. Chem. Soc. Rev. 40, 2644–2672.
Guo, S., Du, Y., Yang, X., Dong, S., Wang, E., 2011. Anal. Chem. 83, 8035–8040.
Guo, Y., Guo, S., Ren, J., Zhai, Y., Dong, S., Wang, E., 2010. ACS Nano 4, 4001–4010.
Guo, Y., Deng, L., Li, J., Guo, S., Wang, E., Dong, S., 2011. ACS Nano 5, 1282–1290.
Guo, Y.J., Li, J., Guo, S.J., 2011. Sens. Actuators B Chem. 160, 295–300.
Guo, Y.J., Han, Y.J., Guo, Y.X., Dong, C., 2013. Biosens. Bioelectron. 45, 95–101.
Hummers, W., Offeman, R.J., 1958. Am. Chem. Soc. 80, 1339.
Joshi, R.K., Gomez, H., Alvi, F., Kumar, A., 2010. J. Phys. Chem. C 114, 6610–6613.
Kim, D.J., Sohn, I.Y., Jung, J.H., Yoon, O.J., Lee, N.E., Park, J.S., 2013. Biosens. Bioelectron. 41, 621–626.
Li, D., Muller, M.B., Gilje, S., Kaner, R.B., Wallace, G.G., 2008. Nat. Nanotechnol. 3, 101–105.
Liu, J., Cao, Z., Lu, Y., 2009. Chem. Rev. 109, 1948–1998.
Loh, K.P., Bao, Q., Eda, G., 2010. Nat. Chem. 2, 1015–1024.
Nierodzik, M.L., Karpatkin, S., 2006. Cancer Cell 10, 355–362.
Ohno, Y., Maehashi, K., Yamashiro, Y., Matsumoto, K., 2009. Nano Lett. 9, 3318–3322.
Orendorff, C.J., Sau, T.K., Murphy, C.J., 2006. Small 2, 636.
Rekharsky, M., Inoue, Y., 1998. Chem. Rev. 98, 1875–1918.
Robinson, J.T., Perkins, F.K., Snow, E.S., Wei, Z., Sheehan, P.E., 2008. Nano Lett. 8, 3137–3140.
Rosi, N.L., Mirkin, C.A., 2005. Chem. Rev. 105, 1547–1562.
Saha, K., Agasti, S.S., Kim, C., Li, X., Rotello, V.M., 2012. Chem. Rev. 112, 2739–2779.
Schedin, F., Geim, A.K., Morozov, S.V., Hill, E.W., Blake, P., Katsnelson, M.I., Novoselov, K.S., 2007. Nat. Mater. 6, 652–655.
Shang, N.G., Papakonstantinou, P., McMullan, M., Chu, M., Stamboulis, A., Potenza, A., Dhesi, S.S., Marchetto, H., 2008. Adv. Funct. Mater. 18, 3506–3514.
Song, S., Wang, L., Li, J., Zhao, J., Fan, C., 2008. Anal. Chem. 27, 108–117.
Song, Y., Qu, K., Zhao, C., Ren, J., Qu, X., 2010. Adv. Mater. 22, 2206–2210.
Tao, Y., Lin, Y.H., Ren, J.S., Qu, X.G., 2013. Biomaterials 34, 4810–4817.
Tian, X., Cheng, C., Yuan, H., Du, J., Xiao, D., Xie, S., Choi, M., 2012. Talanta 93, 79–85.
Tombelli, S., Minunni, M., Mascini, M., 2005. Biosens. Bioelectron. 20, 2424–2434.
Wang, F., Khaledi, M.G., 1996. Anal. Chem. 68, 3460–3467.
Wang, H., Yang, R., Yang, L., Tan, W., 2009. ACS Nano 3, 2451–2460.
Wu, X., Hu, Y., Jin, J., Zhou, N., Wu, P., Zhang, H., Cai, C., 2010. Anal. Chem. 82, 3588–3596.
Wu, Y., Xu, W., Bai, L., Yuan, Y., Yi, H., Chai, Y., 2013. Biosen. Bioelectron. 50, 50–56.
Xu, Z., He, C., Sun, T., Wang, L., 2013. Electroanalysis 25, 2339–2344.
Zhang, Z., Luo, L., Zhu, L., Ding, Y., Deng, D., Wang, Z., 2013. Analyst 138, 5365–5370.
Zhou, M., Zhai, Y., Dong, S., 2009. Anal. Chem. 81, 5603–5613.
Zhao, Q., Li, X.-F., Le, X.C., 2011. Anal. Chem. 83, 9234–9236.